Old data, new forensics: The first second of SN 1987A neutrino emission

Shirley Weishi Li[1,2,*] John F. Beacom[3,4,5,†] Luke F. Roberts[6,‡] and Francesco Capozzi[7,8,§]

[1]*Theoretical Physics Department, Fermi National Accelerator Laboratory, Batavia, Illinois 60510, USA*
[2]*Department of Physics and Astronomy, University of California, Irvine, California 92697, USA*
[3]*Center for Cosmology and AstroParticle Physics (CCAPP),*
Ohio State University, Columbus, Ohio 43210, USA
[4]*Department of Physics, Ohio State University, Columbus, Ohio 43210, USA*
[5]*Department of Astronomy, Ohio State University, Columbus, Ohio 43210, USA*
[6]*Computer, Computational, and Statistical Sciences Division,*
Los Alamos National Laboratory, Los Alamos, New Mexico 87545, USA
[7]*Dipartimento di Scienze Fisiche e Chimiche, Università degli Studi dell'Aquila, 67100 L'Aquila, Italy*
[8]*Istituto Nazionale di Fisica Nucleare (INFN), Laboratori Nazionali del Gran Sasso,*
67100 Assergi (AQ), Italy

The next Milky Way supernova will be an epochal event in multimessenger astronomy, critical to tests of supernovae, neutrinos, and new physics. Realizing this potential depends on having realistic simulations of core collapse. We investigate the neutrino predictions of modern models (1-, 2-, and 3-D) over the first $\simeq 1$ s, making the first detailed comparisons of these models to each other and to the SN 1987A neutrino data. Even with different methods and inputs, *the models generally agree with each other*. However, even considering the low neutrino counts, *the models generally disagree with data*. What can cause this? We show that neither neutrino oscillations nor different progenitor masses appear to be a sufficient solution. We outline urgently needed work.

I. INTRODUCTION

As spectacular as SN 1987A was for multimessenger astronomy—with detections across the electromagnetic spectrum, plus $\simeq 19$ neutrino events [1–6]—the next Milky Way core-collapse supernova should be much more so [7–10]. We have dramatically better sensitivity to neutrinos, a key observable because they carry the dominant energy release and because they probe the dynamics of the inner core. And we have dramatically better sensitivity across the electromagnetic spectrum and to gravitational waves. Because nearby supernovae are rare—about $(2 \pm 1)/$ century [11–13]—we likely have just one chance over the next few decades to get this right.

To interpret the supernova data, numerical simulations of core collapse will be essential. Recently, newly sophisticated approaches—including 3-D, multienergy-group radiation-hydrodynamics models of successful explosions—have become available [14–28]. These models predict explosion properties (e.g., final energies and remnant masses) as well as neutrino signals up to $\simeq 1$ s after core bounce, which is

crucial for assessing explodability and which includes a large fraction of the total emission. However, the readiness of these models for comparison to the next supernova has not been adequately assessed.

In this paper, we tackle two distinct but related problems. Our first goal is to compare models to each other, which gives an estimate of the *modeling uncertainties*. Our second goal is to compare models to the SN 1987A data [1–4], which gives an estimate of the *physical uncertainties*. There is very limited prior work comparing models to each other [18] and models to data [29,30]. What makes the present work possible is advances in the breadth and precision of supernova models, which give us new forensic tools to examine the SN 1987A data.

In the following, we first consider a nominal case of a $20 M_\odot$ (initial mass) single-star progenitor with no neutrino oscillations. This progenitor was initially thought to be appropriate for SN 1987A [5,31] and thus has the broadest set of supernova models. While neglecting neutrino oscillations is not realistic, it matches supernova simulation outputs and is well defined. We allow other aspects of the simulations, including the dimensionality (1-D, 2-D, and 3-D), to vary freely so that we can include all modern predictions [18–28]. Then, to test the impact of changing two key theoretical inputs, we vary the neutrino-oscillation scenario and the progenitor mass. Last, we conclude and

*shirley.li@uci.edu
†beacom.7@osu.edu
‡lfroberts@lanl.gov
§francesco.capozzi@univaq.it

083025-1

discuss actions needed to prepare for the next Milky Way neutrino burst.

In the Appendix, we provide supporting details. Appendix A summarizes key aspects of the supernova models, Appendix B shows the 1987A data we use, Appendix C focuses on how the average energy and spectrum parameter are calculated for each model, Appendix D explains the calculation of the detected positron energy spectra, Appendix E provides details about the statistical tests, Appendix F explains our model selection criteria compared to Ref. [32], Appendix G presents results on progenitor variations, and Appendix H shows details of the oscillation calculations.

II. REVIEW OF SUPERNOVA MODELS

In core-collapse supernovae [33–36], the white-dwarf-like iron core of a massive star collapses to form a protoneutron star (PNS), releasing nearly all of the gravitational binding energy difference, $E_{tot} \simeq (3/5)GM_{PNS}^2/R_{PNS} \simeq 3 \times 10^{53}$ erg, in neutrinos of all flavors with comparable fluences. Neutrinos diffuse out of the hot, dense, neutron-rich PNS, decoupling at the neutrinospheres, with average energies of $\simeq 10$–15 MeV. About half of the total energy is emitted in the first $\simeq 1$ s after core bounce, largely powered by accretion onto the PNS, with the other half released over ~ 10 s, as the PNS cools and deleptonizes. In the neutrino mechanism [37,38], after decoupling from the PNS, a few percent of the early-time neutrinos interact with the collapsing layers of the star outside the PNS, potentially reversing the infall and driving an explosion.

To understand the detailed physics and astrophysics of core collapse, large-scale multidimensional simulations are critical [14–28]. Starting from a preexplosion massive-star progenitor model and choices for the equation of state and neutrino opacities of dense matter, modern simulations evolve the equations of nonequilibrium neutrino transport, (magneto-)hydrodynamics, and gravity for as long as is computationally feasible. In the last decade, the simulation community has made significant progress toward showing the viability of the neutrino mechanism in multidimensional simulations and in predicting the observed properties of supernovae. Nevertheless, these models have shortcomings, including the neglect of neutrino oscillations, significant uncertainties in the progenitor models, often under-resolved hydrodynamic flows, and simulation times of $\lesssim 1$ s after bounce, which misses the PNS cooling phase [39–42].

III. REVIEW OF SUPERNOVA 1987A

Multi-messenger observations of SN 1987A confirmed that a type-II supernova is driven by the collapse of the core of a massive star into a PNS, powering a neutrino burst from the core and a delayed optical burst from the envelope [5,6].

The water-Cherenkov experiments Kamiokande-II (Kam-II) and Irvine-Michigan-Brookhaven (IMB) detected $\simeq 19$ $\bar{\nu}_e$ events in total via inverse beta decay,

$\bar{\nu}_e + p \to e^+ + n$, over $\simeq 10$ s [1–4]. (We neglect the Baksan experiment because it was $\simeq 8$ times smaller than Kam-II and had significant backgrounds [43,44].) Though only one flavor was clearly detected, the results were broadly consistent with basic expectations for the total energy, average neutrino energy, and duration of the neutrino pulse. Theoretical analyses included comparisons to the supernova models of the time [45–47], which were far less sophisticated than those available today.

Observations across the electromagnetic spectrum, at the time and since, have also been critical for understanding the explosion [5,6,48]. Initially, it was thought that the pre- and postsupernova observations were consistent with those expected for a $20M_\odot$ single-star progenitor [49–51]. Later work claimed that a binary-merger scenario is favored [52], though there is no consensus on this. On the one hand, the binary-progenitor models of Ref. [53] suggest that the helium core mass may be substantially smaller—and the envelope mass substantially larger—than the values found for typical single-star progenitors. On the other hand, the binary-progenitor models of Refs. [54,55] suggest that the precollapse structure of the merger remnant is not so different than that predicted for single-star $20M_\odot$ progenitors.

IV. COMPARING MODELS

We first consider the nominal case of a $20M_\odot$ progenitor and no neutrino oscillations. For all modern 1-, 2-, and 3-D models with $20M_\odot$ progenitors [18–28], we collect information on their neutrino fluxes and spectra. We seek to assess the full variation between models, though they are not completely distinct, e.g., many share progenitors [56]. These models vary significantly, but we do not attempt to adjudicate between them. Most multi-D models lead to successful explosions, with explosion times ranging from 0.2–0.8 s. The model details are given in Appendix A.

Figure 1 shows their time profiles of $\bar{\nu}_e$ luminosity and root-mean-square (RMS) energy (other flavors in Appendix C). For the spectra, we assume a commonly used form, $f_\alpha(E_\nu) = \mathcal{N}(E_\nu/\langle E_\nu \rangle)^{\alpha-2}e^{-(\alpha+1)E_\nu/\langle E_\nu \rangle}$, where $\langle E_\nu \rangle$ is the average energy and α sets the spectrum shape [57]. Different groups characterize spectra differently, which we correct for in Appendix C.

To model the detected spectra, we follow standard calculations (e.g., Refs. [58–62]) and give details in Appendix D. The dominant process is $\bar{\nu}_e + p \to e^+ + n$ with free (hydrogen) protons, for which we take the cross sections and kinematics from Refs. [63,64]. To model the detectors, we take into account their fiducial masses, energy resolutions, and trigger efficiencies [1–4]. Because of the different detector responses, the detected positron energies are expected to be significantly lower for Kam-II than IMB. For the distance of SN 1987A, we use 51.4 kpc [65].

We compare the predicted and observed SN 1987A neutrino data using simple, robust observables and statistical tests. We conduct goodness-of-fit tests (computing
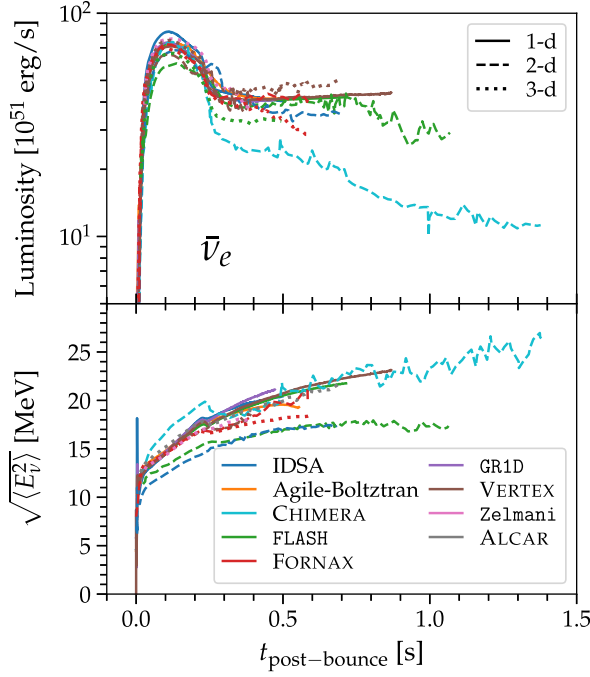
FIG. 1. Neutrino ($\bar{\nu}_e$; others shown in Appendix C) luminosity and RMS energy profiles from supernova simulations [18–28].
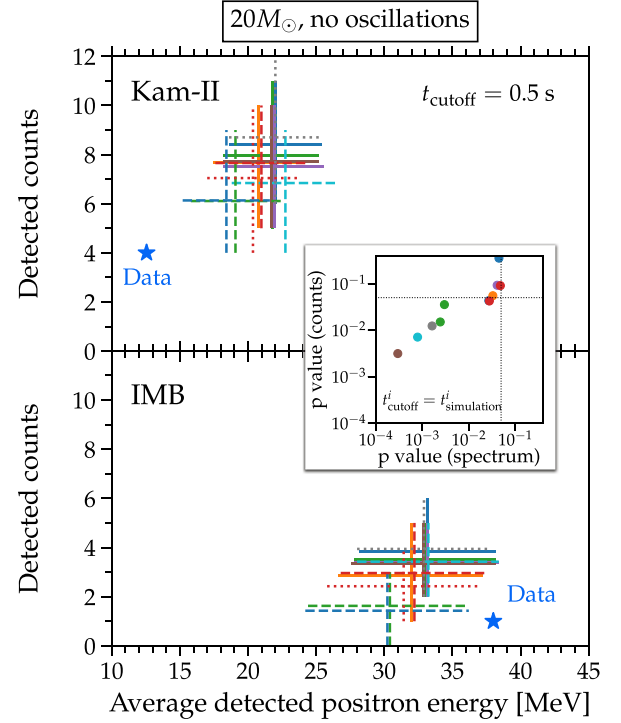

FIG. 2. Predicted counts and average energies of supernova models (colors as in Fig. 1), compared to each other and to SN 1987A data. Our main calculations are in the inset.

p-values) between pairs of models and between each model and the SN 1987A data. *Because we are testing goodness-of-fit, rather than doing parameter estimation, maximum likelihood is not a suitable method; see Appendix E.*

The main panels of Figs. 2–4 show simple visual comparisons of the counts and average detected energies. For consistency, here we cut off all models at 0.5 s. For each model, we forward-model the predicted signals, taking into account properties of the individual detectors and Poisson fluctuations. Because we are assessing *goodness of fit* for many models, we directly calculate $P(\text{data}|\text{model})$ and show the full uncertainties on the models instead of the data.

The insets of Figs. 2–4 show our main statistical calculations. Larger p-values indicate agreement; *a priori*, we defined $p < 0.05$ as indicating inconsistency for a given model, *though our focus is on what happens for the majority of models.* Here, we allow each model to go to its full run time (typically 0.5–1.5 s), considering both the counts in the time profile and the shape of the energy spectrum, which we treat separately, given the short timescale and the low statistics. The spectrum p-value turns out to be the more powerful indicator. For the counts tests, the p-values are the one-sided cumulative Poisson probabilities. For the spectrum tests, we use one-dimensional Kolmogorov-Smirnov statistics, following Monte Carlo modeling of the predicted data. We allow free time offsets between the predictions and the data (core bounce to first event), finding that these values are $\simeq 0.1$ s for Kam-II and $\simeq 0.2$ s for IMB, both small, so this freedom does not affect our results.

V. RESULTS FOR THE NOMINAL CASE

Figure 2 shows the model-to-model comparisons for a $20M_\odot$ progenitor with no neutrino oscillations. The p-values (not shown) obtained by comparing pairs of models range over 0.06–0.52 for the counts (Kam-II and IMB combined) and 0.03–0.99 for the spectra (Kam-II only, as IMB has too few counts). Thus we find general *agreement* among the model predictions. Considering the range and complexity of the inputs and methods in supernova modeling, this agreement is encouraging, though it remains important to understand the residual differences. Also, this agreement is partially due to restricting all models to a short runtime of 0.5 s (see discussion near Fig. 3).

Figure 2 also shows the model-to-data comparisons. A general *disagreement* in both the counts and spectra is evident. The predicted counts are too high for Kam-II and mostly too high for IMB. The predicted average detected energies are too high for Kam-II and slightly too low for IMB. (Because IMB has just one detected event in this time range, we do not use the predicted spectrum in our statistical tests; hence our results do not merely reflect the well-known spectrum tension with Kam-II.) Quantitatively, no model-to-data comparisons have both p-values larger than 0.05, and many are much worse. The two p-values tend to be correlated because the counts depend on $E_{\text{tot}}\langle E_\nu \rangle$; we show both p-values for illustration. The results suggest that an overall cooler neutrino spectrum could explain all of the data
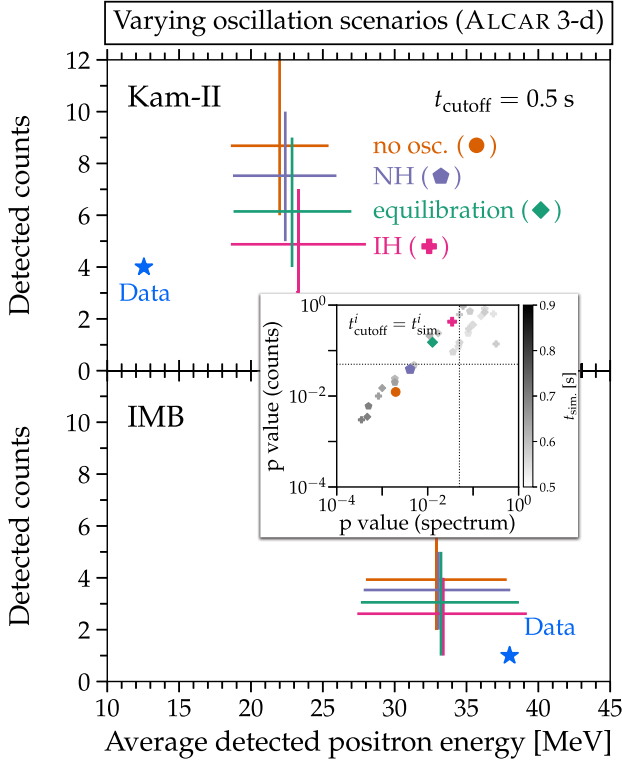
FIG. 3. Similar to Fig. 2, with the theory predictions from the ALCAR 3-D model for $20M_\odot$ [27] and different oscillation scenarios. The simulation cutoff time is 0.68 s. The gray symbols show the p-values from other models (see Appendixes G and H).

except the detected average energy for IMB, which might be accommodated by an enhanced spectrum tail [66,67].

VI. POSSIBLE SOLUTIONS: NEUTRINO OSCILLATIONS

The data are affected by neutrino oscillations [9,68–72], with the effects depending upon differences in the initial neutrino luminosities and spectra, set by differences in their production processes and opacities. The details depend on the high densities of matter and other neutrinos, which are uncertain [9]. Generally, large flavor conversions due to coherent forward scattering on electrons are expected in the stellar envelope [73], while conversions induced by forward scattering of neutrinos among themselves and those induced by inelastic collisions can occur starting from the neutrinospheres [70–72].

We study the effects of oscillations with a few representative cases. Considering only matter-induced effects, if the neutrino mass ordering follows the inverted hierarchy (IH), there can be a nearly complete exchange of the $\bar{\nu}_e$ and $\bar{\nu}_x$ ($\bar{\nu}_\mu$ and $\bar{\nu}_\tau$) flavors, with almost no change for the ν_e and ν_x flavors [73]. In the normal hierarchy (NH), the opposite occurs. With neutrino-induced effects, it is possible to have nearly complete equilibration of all six flavors soon after decoupling, because of rapid flavor conversions induced by

interactions of neutrinos among themselves [70–72]. Further details are in Appendix H.

Figure 3 shows the range of effects for neutrino-oscillation scenarios (for the ALCAR 3-D [27] model and a $20M_\odot$ progenitor, chosen because it is 3-D and has a long runtime). In general, oscillations decrease the predicted counts and increase the average energies, as $\bar{\nu}_x$ has lower fluxes but higher energies than $\bar{\nu}_e$. For most models (including this one), the reduction in flux is more significant. The poor agreement may indicate that neutrino oscillations need to be implemented in supernova simulations [74–76]. Note (see grayscale in inset) that the models with reasonable p-values all have short runtimes.

VII. POSSIBLE SOLUTIONS: SUPERNOVA PROGENITORS

The data are also affected by the choice of progenitor [29,77]. The structure of the star at collapse determines the accretion rate onto the PNS, which strongly influences the neutrino emission. A key question is if models with progenitors other than the $20M_\odot$ single-star cases would better fit the SN 1987A data.

Figure 4 shows the effects of different choices of progenitor mass, using the suite of FORNAX 2-D models [36], chosen because of their wide range of progenitor masses (we use $16-30M_\odot$) and long runtimes. None of the
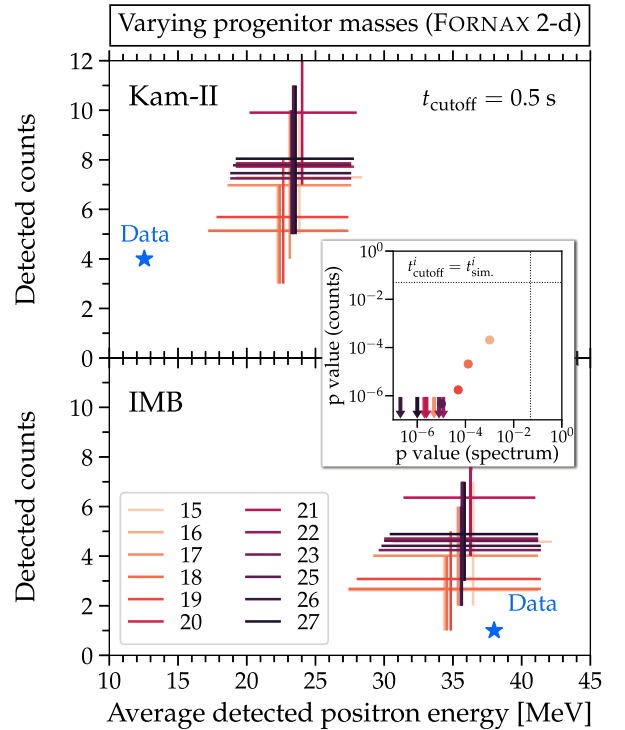

FIG. 4. Similar to Fig. 2, with the theory predictions corresponding to different progenitors from FORNAX 2-D models [36], with no oscillations included.

progenitors provides a good fit to the data. We have also carried out this analysis (see selected results in Appendix G) for the suites of models from Refs. [22,28,78–83], again finding poor agreement with data. We also considered nonisotropic emission [84–87]; however, the predicted changes to the number flux are less than $\pm 20\%$ and those on the average energy are even less, too small to consistently explain the observed discrepancies.

The lack of agreement between models and SN 1987A data may indicate missing physics. Softening the predicted neutrino spectra would require changing the thermodynamic structure of the outer layers of the PNS or changing the neutrino opacity in those regions. However, it may just be that there are not enough models. There are not many studies of the same progenitors with different simulation codes, and there are also not many different progenitors in use. Additionally, binary-merger models for the progenitor of SN 1987A (which do not clearly map onto single-star models) are needed, but only Ref. [55] provides neutrino predictions. A broad range of new simulation work on progenitors and core collapse is needed, especially combining both high sophistication and long runtime. A big step in that direction is made in Ref. [88] (for $19 M_\odot$), but which we find gives a comparably poor match to the SN 1987A data.

VIII. CONCLUSIONS AND WAYS FORWARD

The SN 1987A neutrino and electromagnetic data, which reasonably agreed with supernova models of the time, have been of critical importance to our understanding of core-collapse supernovae. It is commonly assumed that modern supernova models—with 36 years of improvements—also match the data. We revisit this assumption.

We show that modern supernova models (for a $20 M_\odot$ progenitor and no neutrino oscillations) disagree with 1987A neutrino data in the first $\simeq 0.5$–1.5 s, where the highest-precision models end. When we include the effects of neutrino oscillations or vary the progenitor mass, the tension with data changes somewhat but remains. We also show that modern supernova models are in good agreement with each other, which suggests that there may be a common solution to the disagreement with SN 1987A data, perhaps even one that also improves explosion energies in simulations. There is a range of possibilities, including that our implementation or even understanding of the physics in the simulations is incomplete, that not enough progenitor models have been considered, that the initial neutrino spectra are significantly nonthermal, or that neutrino oscillations need to be directly implemented in supernova simulations. Separately, it would also be interesting to reanalyze the raw data from both detectors, using

present detector-modeling and event-reconstruction techniques, both vastly improved over those from 36 years ago.

To realize the full potential of the signals from the next Milky Way supernova, the community will ultimately need a set of modern models that agree (for the same progenitor mass) with each other and the neutrino and electromagnetic data. Confidence in this would greatly increase if the same were achieved for SN 1987A. Reaching these goals should be pursued with urgency. It is especially important that multi-D supernova simulations push their run times out to a few seconds, beyond which PNS cooling simulations may be adequate.

Note added. A few months after our work appeared on arXiv, Ref. [32] appeared, also investigating how modern supernova simulation predictions compare to 1987A neutrino data. We discuss this paper in Appendix F.

APPENDIX A: SUPERNOVA SIMULATIONS

Table I summarizes the list of supernova models employed in this work. The p-values are computed up to the maximum time in each simulation. We exclude four models from our statistical tests: the 1-D FORNAX models from Ref. [18] that have a known bug [89], a FLASH 3-D simulation paper [26] that reports neutrino luminosities but not average energies, and the PROMETHEUS-VERTEX 2-D [22] and Zelmani 3-D [25] simulations, which only run to 0.38 s.

TABLE I.   A summary of the supernova simulations considered. The progenitor mass refers to the zero-age main sequence mass. We take the explosion time to be the moment when the mean shock radius reaches 500 km. The p-values are obtained from the comparison between the model predictions and SN 1987A data. The p-values in the counts column are from comparing the total number of events in Kam-II and IMB. Those in the spectrum column are from comparing the cumulative spectrum distribution in Kam-II only (because IMB has too few counts). See the text for why some models do not have p-values.

Code	Dimension	Progenitor Mass [$M_\odot$]	Explosion	t_{exp} [s]	t_{sim} [s]	p-value (counts)	p-value (spectra)	References
3DnSNe-IDSA					0.50	0.043	0.027	
AGILE-BOLTZTRAN					0.55	0.055	0.034	
FLASH-M1	1-D	20 [56]	N/A	N/A	0.71	0.015	0.002	O'Connor et al. [18]
FORNAX					1.10	$\cdots$	$\cdots$	
GR1D					0.47	0.092	0.043	
PROMETHEUS-VERTEX					0.87	0.003	3×10^{-4}	
CHIMERA	2-D	20 [56]	Yes	0.21	1.37	0.007	7×10^{-4}	Bruenn et al. [19,20]
FLASH	2-D	20 [56]	Yes	0.82	1.06	0.035	0.003	O'Connor et al. [21]
PROMETHEUS-VERTEX	2-D	20 [56]	Yes	0.36	0.38	$\cdots$	$\cdots$	Summa et al. [22]
IDSA	2-D	20 [56]	Yes/No	0.4–0.6	0.68	0.35	0.047	Kotake et al. [23]
FORNAX	2-D	20 [56]	No	N/A	0.58	0.042	0.029	Vartanyan et al. [24]
Zelmani	3-D	20 [56]	Yes	0.38	0.38	$\cdots$	$\cdots$	Ott et al. [25]
FLASH	3-D	20 [90]	No	N/A	0.50	$\cdots$	$\cdots$	O'Connor et al. [26]
ALCAR	3-D	20 [56]	No	N/A	0.68	0.012	0.002	Glas et al. [27]
FORNAX	3-D	20 [91]	Yes	0.45	0.59	0.091	0.047	Burrows et al. [28]

APPENDIX B: SN 1987A DATA

Tables II and III show the 1987A events in Kam-II and IMB that we used in this work. Note that there are later detected events that we did not include because they are after the longest simulation time that we consider, $\simeq 4.6$ s.

APPENDIX C: NEUTRINO ENERGY SPECTRA AND LUMINOSITIES

Figure 5 shows the time evolution of luminosity and root-mean-square (RMS) energy for all flavors and for each

TABLE II.   Kam-II data taken from Ref. [2]. The event energy is the total energy of the detected positron.

Event	Time [s]	Energy [MeV]
1	0.000	20.0
2	0.107	13.5
3	0.303	7.5
4	0.324	9.2
5	0.507	12.8
6	1.541	35.4
7	1.728	21.0
8	1.915	19.8

model. It is evident by eye that there is relatively good agreement, with some exceptions. Most of these quantities are taken directly from publications, but some require a conversion from average energies, $\langle E_\nu \rangle$, to root-mean-square energies, $\sqrt{\langle E_\nu^2 \rangle}$. Some require changing from the fluid frame to an infinite observer frame.

Our calculations require the full neutrino energy distribution function, $f(E_\nu)$, which is assumed to be already integrated over neutrino propagation angle. Sometimes the output $f(E_\nu)$ from a given model is publicly released, usually in the form of large numerical tables. However, this is available only for very few models. Fortunately, in Ref. [57], a good analytical approximation for $f(E_\nu)$ has

TABLE III.   IMB data taken from Ref. [4]. The event energy is the total energy of the detected positron.

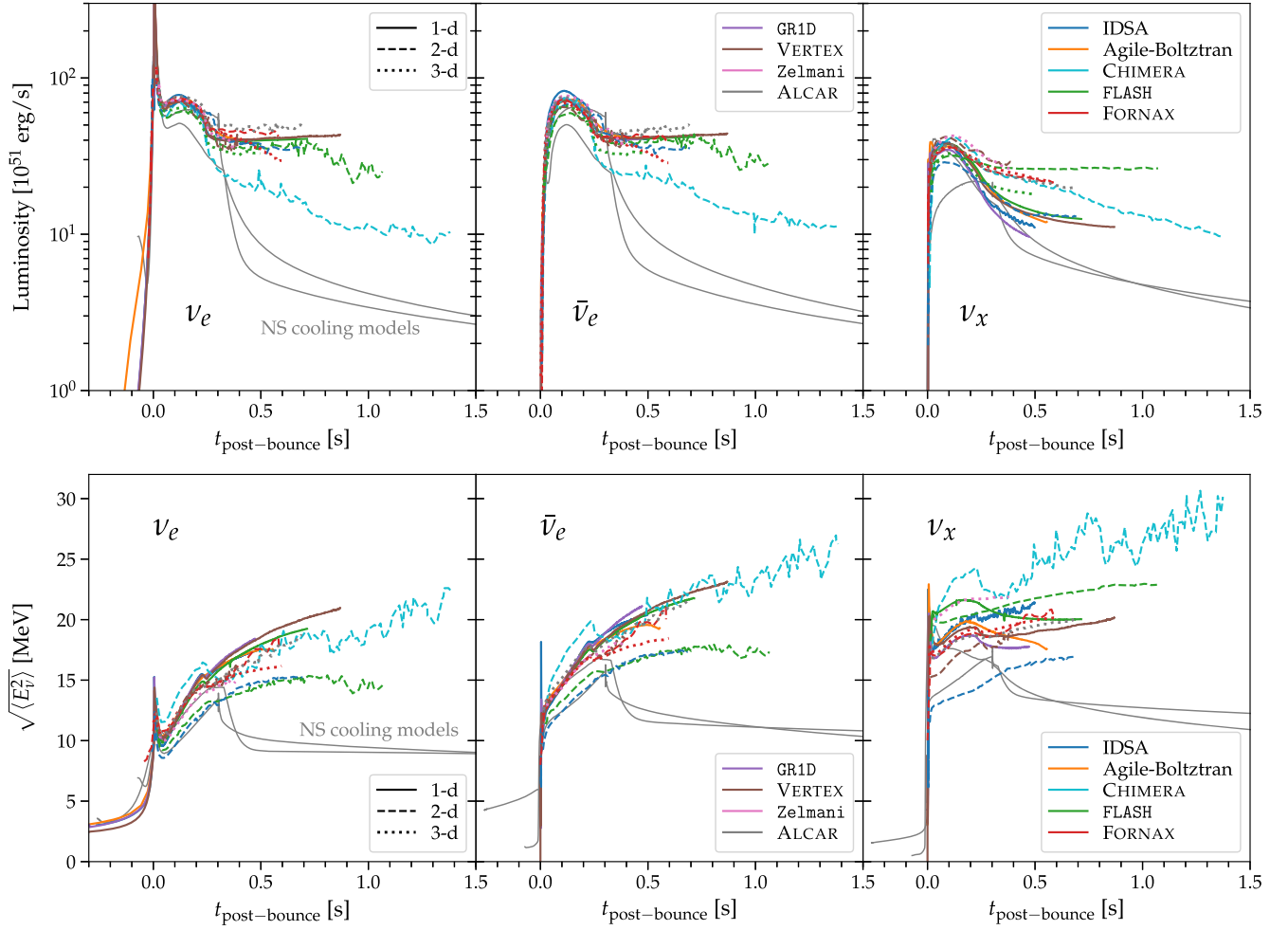| Event	Time [s]	Energy [MeV]
1	0.000	38
2	0.412	37
3	0.650	28
4	1.141	39
5	1.562	36
6	2.684	36

FIG. 5. Neutrino luminosities (top) and RMS energies (bottom) of ν_e, $\bar{\nu}_e$, and ν_x from numerical simulations. The neutronization burst luminosity goes up to $\simeq 5 \times 10^{53}$ erg/s. The ν_x luminosity is shown for only one of the four flavors. The two PNS cooling models are from Refs. [40,92].

been found (we include the E_ν^2 factor in the phase-space integral, not the distribution function):

$$f(\alpha, E_\nu) = \mathcal{N} \left(\frac{E_\nu}{\langle E_\nu \rangle} \right)^{\alpha - 2} e^{-\frac{(\alpha+1)E_\nu}{\langle E_\nu \rangle}}, \qquad (C1)$$

where $\langle E_\nu \rangle$ is the average neutrino energy, defined as

$$\langle E_\nu \rangle = \frac{\int_0^\infty dE_\nu E_\nu^3 f(E_\nu)}{\int_0^\infty dE_\nu E_\nu^2 f(E_\nu)}, \qquad (C2)$$

and α, representing the amount of spectrum pinching, is defined as

$$\frac{\langle E_\nu^2 \rangle}{\langle E_\nu \rangle^2} = \frac{2 + \alpha}{1 + \alpha}, \qquad (C3)$$

and $\mathcal{N}$ is a normalization factor that ensures the distribution function integrates to the local neutrino number density. For a Fermi-Dirac distribution with zero chemical potential, we have $\langle E_\nu \rangle \simeq 3.15T$, where T is the temperature, and $\sqrt{\langle E_\nu^2 \rangle} = 1.14 \langle E_\nu \rangle$.

The pinched spectrum $f(\alpha, E_\nu)$ defined in Eq. (C1) is what we use to calculate the theoretical predictions for SN 1987A. We need both $\langle E_\nu \rangle$ and $\sqrt{\langle E_\nu^2 \rangle}$, but some models only provide one of them, either through numerical tables or figures. To solve this lack of information, we fit for a simple relation between $\langle E_\nu \rangle$ and $\sqrt{\langle E_\nu^2 \rangle}$ using the models that provide both. Figure 6 shows $\sqrt{\langle E_\nu^2 \rangle}$ as a function of $\langle E_\nu \rangle$ for these models. Most models predict $\sqrt{\langle E_\nu^2 \rangle}$ to be between $1.08 \langle E_\nu \rangle$ and $1.13 \langle E_\nu \rangle$ in the energy range 12–20 MeV, where the average energies of most models fall. Thus, we adopt the following relation between average and root-mean-square neutrino energy

$$\sqrt{\langle E_\nu^2 \rangle} = 1.025 \langle E_\nu \rangle + 0.005 \langle E_\nu \rangle^2, \qquad (C4)$$

which fits most of the models well, and is at most 10% away from the FORNAX results. Equation (C4) is then used to compute a relation between α and $\langle E_\nu \rangle$.
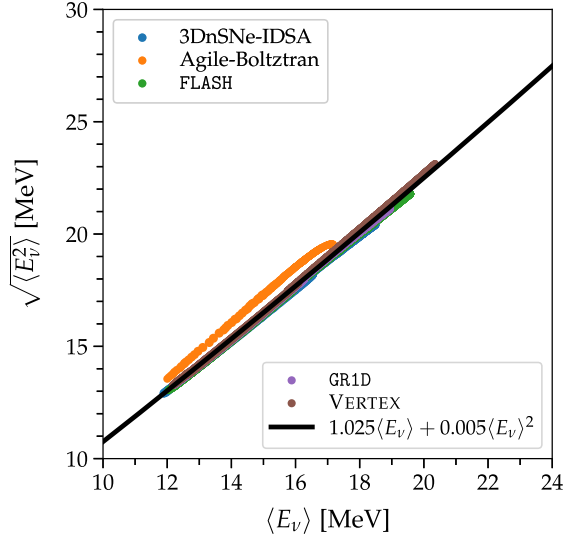
FIG. 6. $\sqrt{\langle E_\nu^2 \rangle}$ as a function of $\langle E_\nu \rangle$ obtained from the numerical simulations where both are provided. The black line is the relation we use in this work.

Note that some groups define $E_{\rm rms} = \sqrt{\langle E_\nu^3 \rangle / \langle E_\nu \rangle}$ as opposed to $E_{\rm rms} = \sqrt{\langle E_\nu^2 \rangle}$. We find that taking this into account leads to negligible changes to the predicted event rates, so we interpret all RMS energies as $\sqrt{\langle E_\nu^2 \rangle}$.

Some models provide neutrino predictions in the comoving frame of the stellar fluid. However, we need quantities defined in the laboratory frame. We use the transformations between these frames from Ref. [23]. For the neutrino luminosity, the transformation reads:

$$L_\nu = L_\nu^{\rm fluid}(1 + v_r/c)/(1 - v_r/c), \qquad \text{(C5)}$$
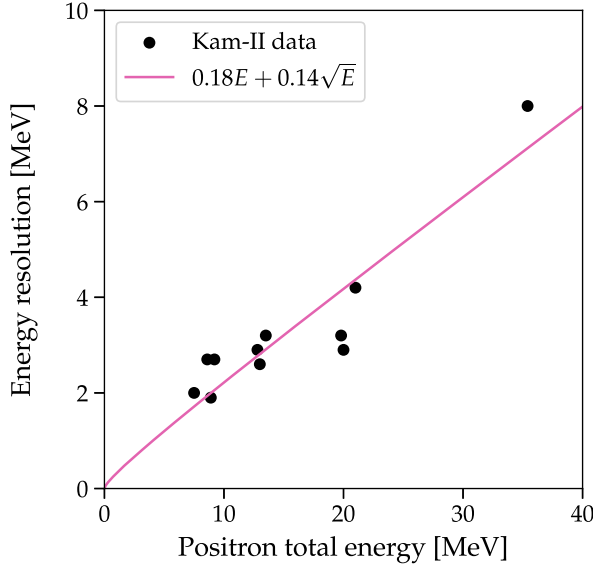
and for the average energy, it is

$$\sqrt{\langle E_\nu^2 \rangle} = \sqrt{\langle E_\nu^2 \rangle^{\rm fluid}}(1 + v_r/c)/\sqrt{1 - (v_r/c)^2}, \quad \text{(C6)}$$

with v_r being the radial velocity and c the speed of light. In Ref. [23], it is assumed $v_r = -0.06c$, which is the average infall velocity at 500 km over the entire 250 ms post bounce. Considering that the transformation between frames is at the level of $O(10\%)$, our approximation can be safely applied to all models.

APPENDIX D: DETECTED POSITRON ENERGY SPECTRUM

We follow the standard approach to compute the positron spectrum [58–62]. As a first step to predicting the detected positron energy spectrum, we calculate the spectrum as a function of the true positron total energy E_+:

$$g(E_+) \propto \int dE_\nu E_\nu^2 f(\langle E_\nu \rangle, \alpha) \frac{d\sigma_{\rm IBD}(E_\nu, E_+)}{dE_+}, \qquad \text{(D1)}$$

where $d\sigma_{\rm IBD}/dE_+$ is the differential cross section for the inverse beta decay [63,64] and $f(\langle E_\nu \rangle, \alpha)$ is defined in Eq. (C1).

To turn $g(E_+)$ into an observed spectrum, we need to convolve it with the detector energy resolution and efficiency. We detail the Kam-II case. The trigger has a threshold of $N_{\rm hit} \geq 20$ (the number of hit photomultiplier tubes), which is equivalent (on average) to a detected energy, $E_{\rm det}$, of 7.5 MeV. The detected spectrum is then
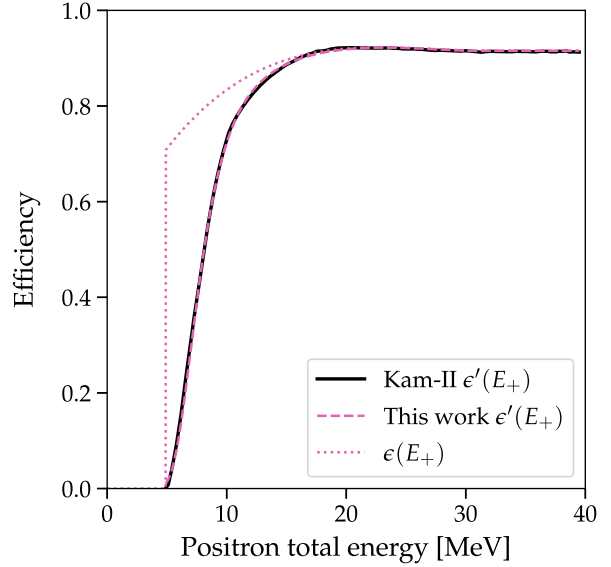

FIG. 7. Left: the black dots represent the energy uncertainty for each event detected in Kam-II, whereas the continuous line is a fit to this data; we use the fit to get the width of the Gaussian energy resolution function defined in the text. Right: the efficiency of Kam-II as a function of the true positron total energy. Note that our calculation perfectly overlaps the line provided by Kam-II.
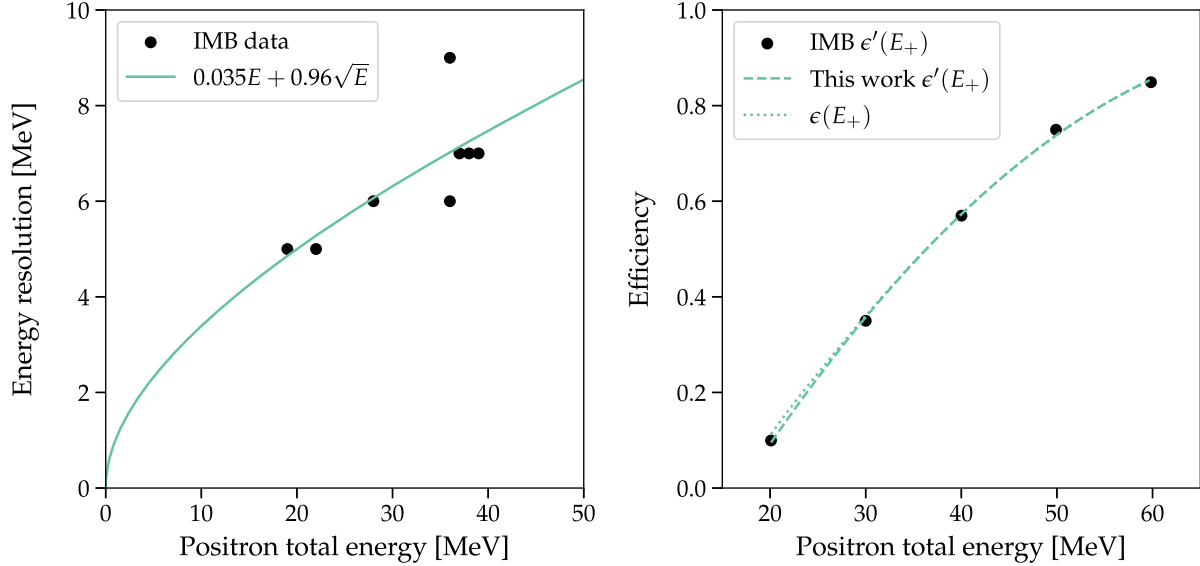
FIG. 8. Same as Fig. 7, but for IMB, which only provides efficiencies at a few energy points.

$$N(E_{\text{det}}) \propto \int dE_+ g(E_+)\epsilon(E_+)R(E_{\text{det}}, E_+)\theta(E_{\text{det}} - 7.5),$$

$$\text{(D2)}$$

where $\epsilon(E_+)$ is the intrinsic detector efficiency (not taking into account the E_{det} cut), $R(E_{\text{det}}, E_+)$ is the energy resolution function and $\theta(E_{\text{det}} - 7.5)$ is the Heaviside step function. We assume $R(E_{\text{det}}, E_+)$ to be a Gaussian function, with the width σ_R having the form $aE_+ + b\sqrt{E_+}$, where the second term arises from the Poisson fluctuations on N_{hit}, while the first term roughly accounts for systematics. The black dots in Fig. 7 (left panel) represent the energy errors of each event detected in Kam-II [2]. We obtain the following expression for the width from a functional fit:

$$\sigma_R^{\text{KamII}}(E_+) = 0.18E_+ + 0.14\sqrt{E_+}. \quad \text{(D3)}$$

The published trigger efficiency curve from Fig. 3 of Ref. [2] should be interpreted as $\epsilon'(E_+)$, combining the intrinsic detector efficiency and the trigger cut:

$$\epsilon'(E_+) = \epsilon(E_+)\int dE_{\text{det}}R(E_{\text{dec}}, E_+)\theta(E_{\text{det}} - 7.5). \quad \text{(D4)}$$

Figure 7 (right panel) shows the trigger efficiency we have computed (pink dashed line) in comparison with the one published by Kam-II (black solid line), which match perfectly. In addition, we also show the inferred intrinsic efficiency $\epsilon(E_+)$ with the dotted line.

A similar procedure has been applied for IMB. Figure 8 displays both the energy resolution (left panel) and the efficiency (right panel) extracted for this experiment.

APPENDIX E: STATISTICAL METHODS

1. Calculating the time offset

As the supernova neutrinos reach Earth, the expected number of events increases as a function of time because the supernova signal is rising. However, due to the limited statistics, the first detected event is generally expected to occur at 0.1–0.2 s after the neutronization burst peak. In addition, because the two detectors, KamII and IMB did not record the absolute time difference of their respective first events, this time offset has to be applied separately to KamII and IMB.

The method we use for calculating the offset time is the following. First, we look only at data as a function of time, and we discard energy information. For example, let us consider one simulation running up to 0.6 s. Let us also assume that KamII data has the following detection times for each event: $(0.0, 0.1, \ldots, t_n)$ s. We test offsets in the range $[0, 0.5]$ s. For every offset (t_0), the detection times with respect to the arrival of the neutronization peak, which can be taken as $t = 0$ in simulations, become $(0.0 + t_0, 0.1 + t_0, \ldots, t_n + t_0)$. Next, we compute the p-value as $P_1 \times P_2$, where P_1 is the Poisson probability of predicting N events and getting N' events, i.e., what we quote as the p-value for rates. P_2 is the Kolmogorov-Smirnov test p-value obtained by comparing the detected and predicted temporal shapes (see Fig. 9 left panel for the spectrum example). We get an array of p-values, one for each value of t_0. We choose the time offset for which the p-value is maximal. In general, in the plausible range of time offset, i.e., $[0.1, 0.2]$ s, the p-value is rather constant because the data is sparse, and we are not including more events to KamII data when shifting the time. Concerning IMB, the number of events can change for some models, which we do use when computing p-values. However, their number would still be so low that their contribution to the combined p-value is only marginal.
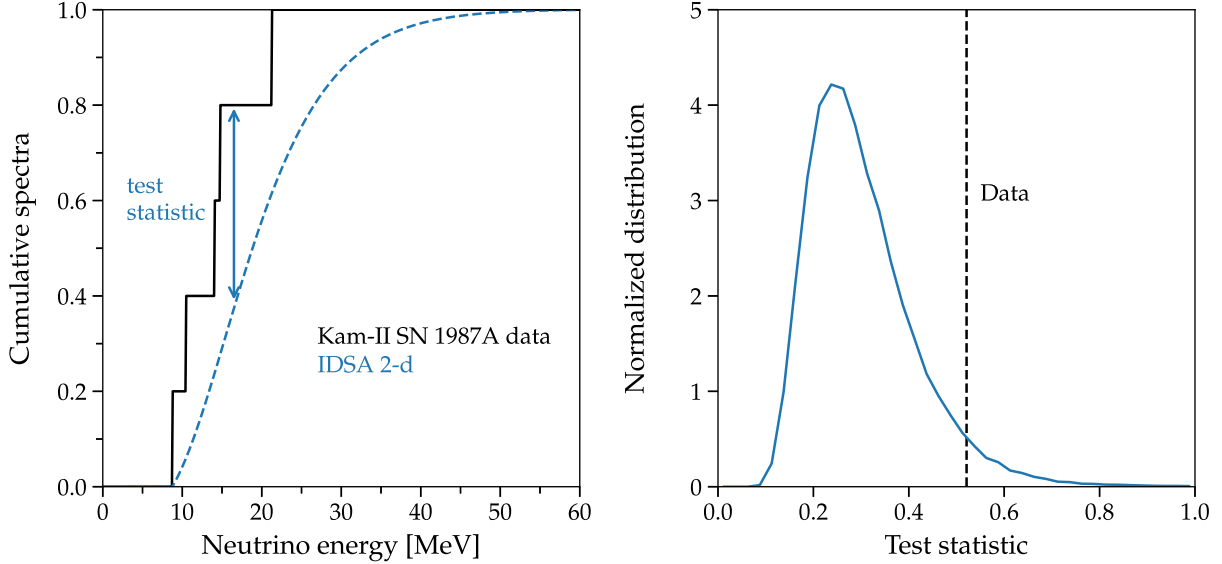
FIG. 9. A demonstration of p-value calculation. Left: the cumulative energy distribution of the IDSA 2-D model and 1987A data and the corresponding test statistic. Right: the test statistic distribution.

2. Cumulative distributions and Kolmogorov-Smirnov tests

To compute the p-values for the spectrum shape, we use a Kolmogorov-Smirnov test. Figure 9 (left panel) illustrates the test statistic. We use one specific model, IDSA 2-D [23], as a concrete example. First, we utilize all the available information and set t_{cutoff} to be the simulation run time, 0.67 s for this model. We then integrate the energy spectrum up to t_{cutoff} and plot the cumulative distribution (blue dashed line). Next, we cut the 1987A Kam-II data also at t_{cutoff}, allowing a variable offset time. The black steps show the cumulative spectrum of the data within 0.67 s. The test statistic is the maximum vertical distance between these two curves, TS_0.

To compute p-values, we run Monte Carlo simulations of each detector to build the test statistic distribution, shown in Fig. 9 (right panel). For this model, we sample many realizations of the data, letting both the total counts and the energy points vary, and compute the test statistic between the model and each realization. The p-value is determined by the fractional area of the p-value distribution more extreme than TS_0.

This Monte Carlo sample is also used to compute the error bars in Figs. 2–4. The vertical error bars follow Poisson fluctuations, as expected. The horizontal error bars are the standard deviation of the mean for the detected positron energies in each detector. As noted in the main text, the results shown in the main panels of those figures are simple visual comparisons, with the insets showing our full statistical calculations.

Figure 10 (top panel) shows how the cumulative counts for the models compare to 1987A data. The green shading indicate smearing over all models, including those for different oscillation scenarios and progenitor masses in Ref. [82]. Here we clearly see the trend of models

predicting too high of event counts throughout the entire 1 s. Figure 10 (bottom panel) shows the cumulative energy spectra of all models, and similarly, the green shading indicate the model range.

One may be tempted to use likelihood as a test statistic to compute p-values. Here we follow the discussions in Ref. [93] (Chapter 11) and explain why this is not a robust statistical procedure. The essential point is that we are doing a goodness-of-fit test. While maximum likelihood is a good method for parameter estimation, it does not work as a goodness-of-fit test, regardless of whether one works in the frequentist or Bayesian framework. A simple demonstration of why is to consider a uniform distribution $h(x) = 1$ between (0, 1), where we want to test whether some random numbers $\{x_i\}$ are drawn from this distribution. Clearly any dataset would generate a likelihood of 1, so this fails as a goodness-of-fit test. The lesson is generically applicable to other distributions because we can always transform a smooth distribution to a uniform one by changing variables. Attempts at goodness-of-fit tests with maximum likelihood thus give different results depending on if one uses x, $\log x$, or another choice as the dependent variable. This model dependence renders the results uninformative.

APPENDIX F: MODEL SELECTION COMPARED TO FIORILLO *et al.*

A few months after our work appeared on arXiv, Ref. [32] appeared, also investigating how modern supernova simulation predictions compare to 1987A neutrino data. We view this paper as largely complementary, as we focus on explosion models (only available at early times) while they focus on PNS cooling models (most suitable for late times) and statistical tests of the complete signal, which seems to be dominated by late times.

$20 M_\odot$, no oscillations
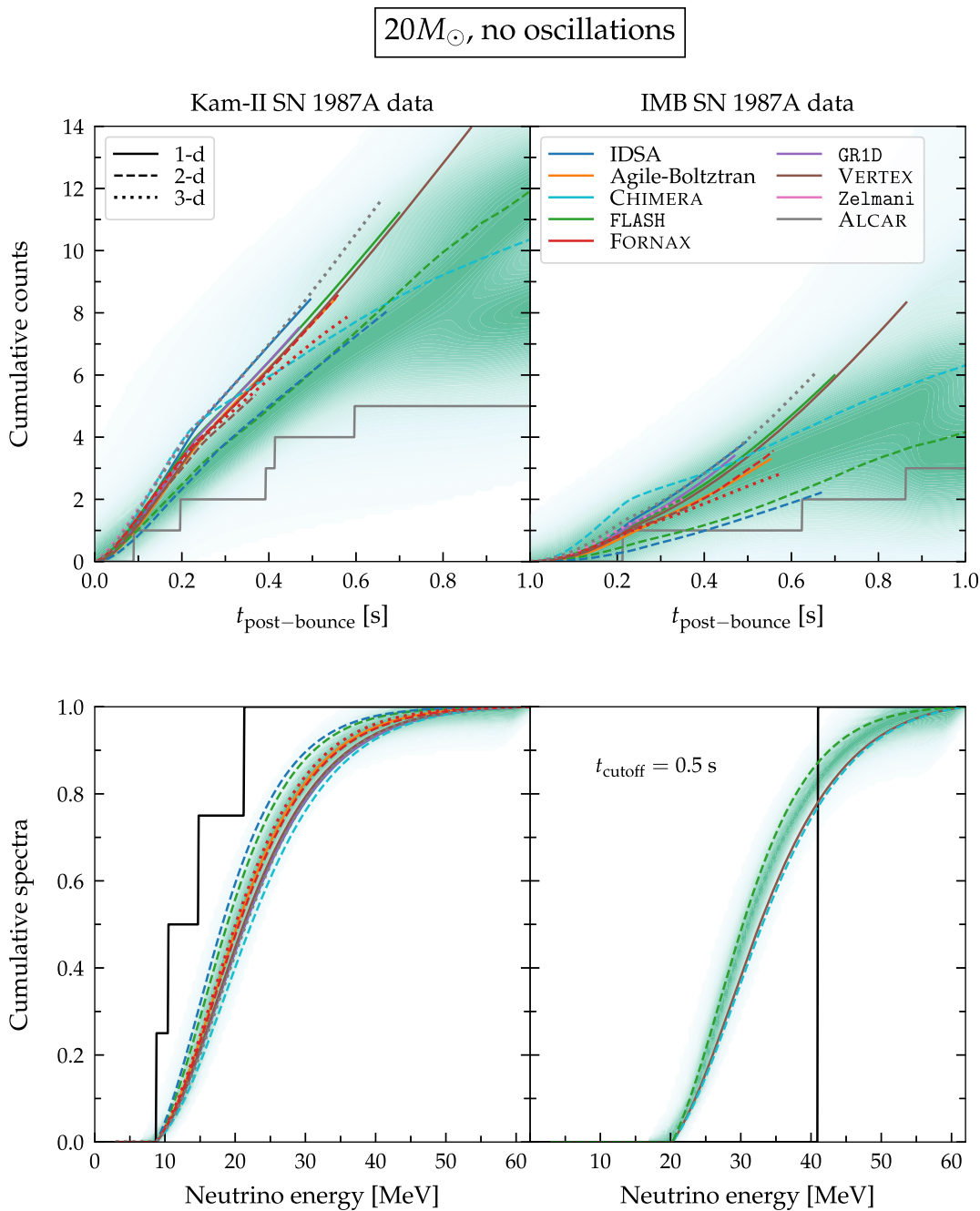
Kam-II SN 1987A data   IMB SN 1987A data

FIG. 10. Cumulative counts (top panel) and cumulative spectra (bottom panel) of models compared to SN 1987A data. The green shading shows the density of all models considered in this work, including the alternative scenarios with neutrino oscillation and different progenitor masses.

Reference [32] also comments on the early time signals, claiming that there is no tension between modern simulations and the 1987A neutrino data, in contrast to our results. Even though there are differences in the treatments regarding experimental data, statistical procedure, etc., we think the crucial difference between the two groups is in the supernova simulations considered. We explain this point here.

Figure 11 shows that the nominal models in Ref. [32] *have much lower luminosities (and significantly lower*

average energies) than the models we consider. This immediately brings their theoretical predictions for the detected signals closer to the early time SN 1987A data, which are dominated by the KamII data.

The main reason for this difference in luminosities and average energies is that we consider models focused on the explosion phase and, therefore, consider primarily the results of 2- and 3-D simulations (although we also compare to the results of 1-D simulations). In contrast,
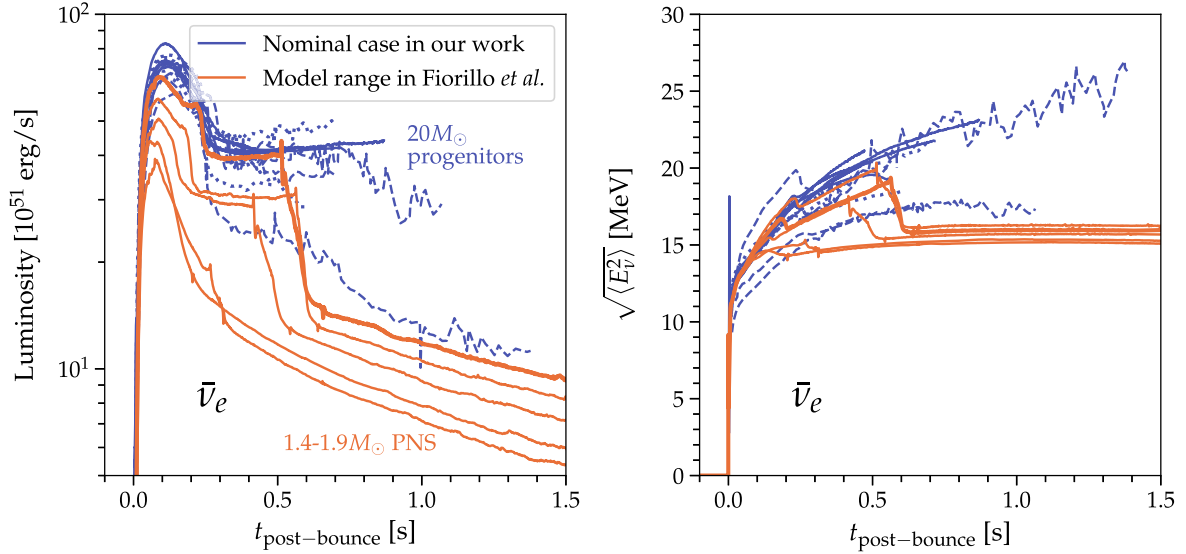
FIG. 11.   Comparison of supernova models: the 1-, 2-, 3-D models used in our work (purple lines; see Fig. 1) and the 1-D models used in Ref. [32] (orange lines, corresponding to various PNS masses). From bottom to top at a time of 1.0 s, these are 1.36, 1.44, 1.62, 1.77, and $1.93 M_\odot$; we show the $1.93 M_\odot$ case with a thick line. These correspond to progenitor masses of 9.0, 18.8, 18.6, 27, and $20 M_\odot$ (note that the order is nonmonotonic); we show the $20 M_\odot$ case with a thick line. *Note that in their fits they emphasize models with substantially lower neutrino luminosities (and somewhat lower average energies) than found in the multi-D models we consider, either because their models employ progenitors that give intrinsically lower luminosities or because they are artificially cut off accretion near 0.6 s by their explosion prescription.*

Ref. [32] considers only 1-D models, which are most suited for studying the PNS cooling phase. Because these 1-D models do not naturally explode, an explosion must be artificially imposed to prevent collapse to a black hole and have the models give a long-term neutrino signal. In Ref. [32], they trigger explosions by removing most of the infalling material outside of the supernova shock at a prescribed time after bounce. As a result, the mass of the PNS in their models and the time of shock runaway are determined by this tunable parameter. Abruptly shutting off accretion by removing most of the outer layers of the star causes the neutrino luminosity to drop rapidly, which is evident in Fig. 11.

For the five luminosity profiles from Ref. [32], as shown in Fig. 11, two are significantly lower than ours at all times, making them closer to the Kam-II data. For one of these profiles, the progenitor mass is very small ($9 M_\odot$). For the other three profiles, while the initial luminosities are more like ours, they drop precipitously in the first second, the time period we focus on, again making the predicted counts closer to the Kam-II data and rather unlike what is expected from most of the 2- and 3-D models.

APPENDIX G: PROGENITORS FROM DIFFERENT GROUPS

In Fig. 4, we show a comparison between model predictions and data for different values of the progenitor

mass, but only for FORNAX 2-D. Here we provide further details.

Figure 12 shows the cumulative distributions for different progenitors by FLASH 1-D [82] compared to 1987A data [83]. This is the study with the largest suites of progenitor models. Because of the huge number of models, we decide not to label any specific progenitors but rather focus on some general points. First, there are clearly two families of curves, one with steeply rising event rates and one with flattening event rates beyond $\simeq 0.5$ s. The first family corresponds to models where the supernova failed to explode and the second to successful explosions. Interestingly, models with successful explosions are thus closer to the SN 1987A data. *This means there may be a strong connection between the two questions "Does the model explode?" and "Does the model match the data?"* Further exploration of that conjecture is needed.

Combining results from all groups with long-term simulations for a range of progenitor models, Fig. 13 (left panel) shows how the p-values for the energy spectrum for FLASH [82], VERTEX [22] and FORNAX [36] change with the progenitor mass in $10 - 80 M_\odot$. This panel assumes a cutoff time of $t_{\text{cutoff}} = 0.5$ s. In this case, most of the p-values lie above the dashed line that represents our $p = 0.05$ threshold. Then most of these models appear to be in agreement with data, especially in the range $10 - 20 M_\odot$. On the other hand, the right panel uses $t_{\text{cutoff}} = 1.3$ s. In this case, a general disagreement with

data is clearly visible. We stress that the choice of $t_{cutoff} = 0.5$ s is only to make the time range for each simulation equal. It is unsurprising that restricting the time range lessens the statistical tension. The p-values for the case where t_{cutoff} is equal to the cutoff time of each simulations are the ones to be taken as references, since ultimately we would like all simulations to agree with data for the entire duration of the neutrino burst.
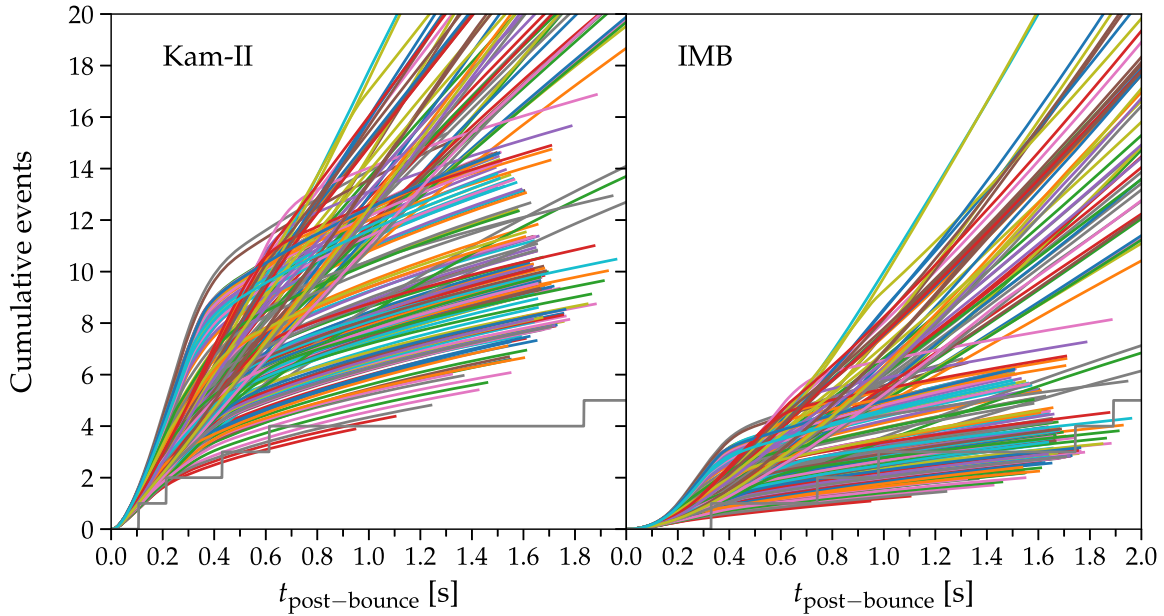

FIG. 12. Cumulative numbers of events for different progenitors simulated with FLASH 1-D [82].
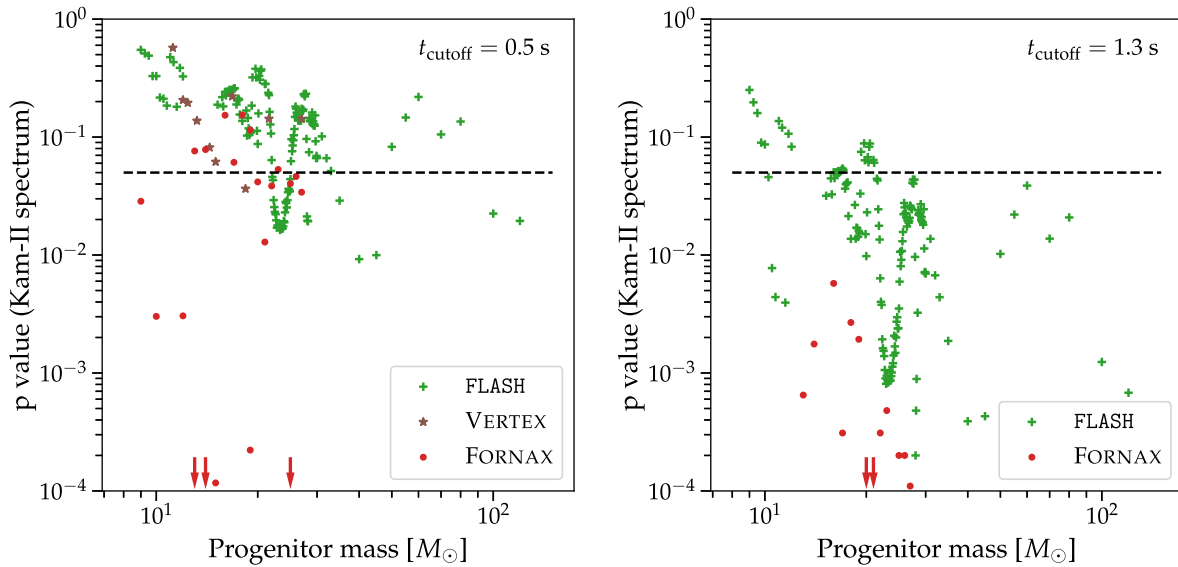

FIG. 13. The p-values obtained through an energy spectrum comparison with Kam-II data for different progenitors masses, simulated with FLASH [82], VERTEX [22], and FORNAX [28,36,78–81], with a cutoff time of 0.5 s (left) and 1.3 s (right).

APPENDIX H: SUPERNOVA NEUTRINO OSCILLATION TREATMENT

We consider a few illustrative oscillation scenarios in the main text, focusing on exploring the possible impact of oscillations on the model-data comparison. We use the following equation for calculating the oscillated flux $\tilde{f}_{\bar{\nu}_e}$ of $\bar{\nu}_e$ as a function of the unoscillated fluxes.

$$\tilde{f}_{\bar{\nu}_e} = f_{\bar{\nu}_e} P(\bar{\nu}_e \to \bar{\nu}_e) + f_{\bar{\nu}_x}[1 - P(\bar{\nu}_e \to \bar{\nu}_e)], \quad \text{(H1)}$$

where $P(\bar{\nu}_e \to \bar{\nu}_e) = \cos^2\theta_{12} \simeq 0.7$ in NH, $P(\bar{\nu}_e \to \bar{\nu}_e) = 0$ in IH and $P(\bar{\nu}_e \to \bar{\nu}_e) = \frac{1}{3}$ for flavor equilibration.

In Figs. 14–17, we show the effects of oscillations on the predicted event rates, spectra, and p-values for models from different groups. For simulations with the same dimensions, we sort the results in ascending order of simulation time. While some models have reasonable p-values, in general the fit worsen as the simulation time increases; when the runtimes are short, models can appear better than they likely are. This point seems to be confirmed by the results of Ref. [88] (for $19M_\odot$), a sophisticated model with a long runtime, which also gives a poor match to the SN 1987A data. It would be desirable to have more models that

run longer. Finally, the goal is to have nearly all models fit the data well.

The p-values for counts and spectra tend to be correlated. The most basic reason is that the detected average energy depends on the neutrino average energy $\langle E \rangle$ and the counts depends on $E_{tot}\langle E \rangle$. There is also a nontrivial interplay in the p-values. As an example, let us consider the ALCAR 3-D results, as shown in the main text in Fig. 3. Oscillations convert $\bar{\nu}_x$ and $\bar{\nu}_e$ into each other, which means that the detected $\bar{\nu}_e$ spectrum has a lower number of neutrinos and an increased average energy with respect to the one at production. Because without oscillations theoretical predictions give a higher flux compared to data, their inclusion makes the counts p-value better. On the other hand, the unoscillated value of the average energy for $\bar{\nu}_e$ is higher than that the observed one in the Kam-II data, thus oscillations should, in principle, make the spectrum p-value worse. But the opposite happens because the spectrum p-value includes information on counts in a subtle way. To explain why, let us look at Fig. 9. If we increase the predicted average energy, the predicted spectrum (blue dashed line in the left panel) shifts to the right, increasing the test statistic relative to data. However, to calculate a p-value for a test statistic, we run Monte Carlo samples based
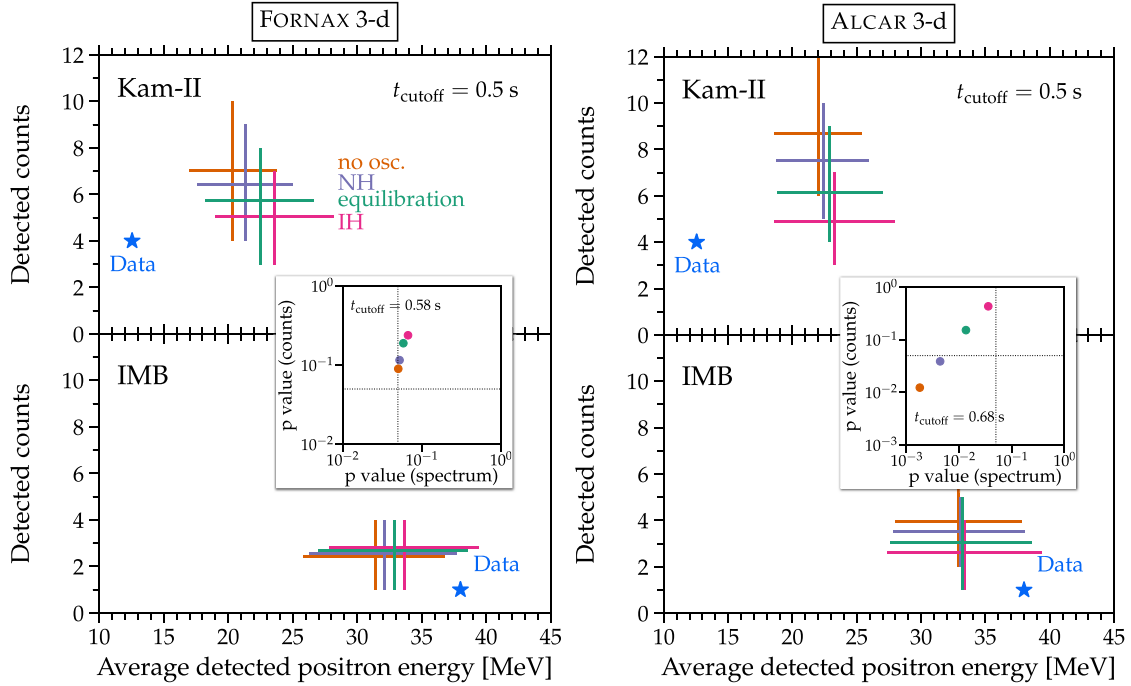

FIG. 14. Different oscillation scenarios for 3-D simulations.
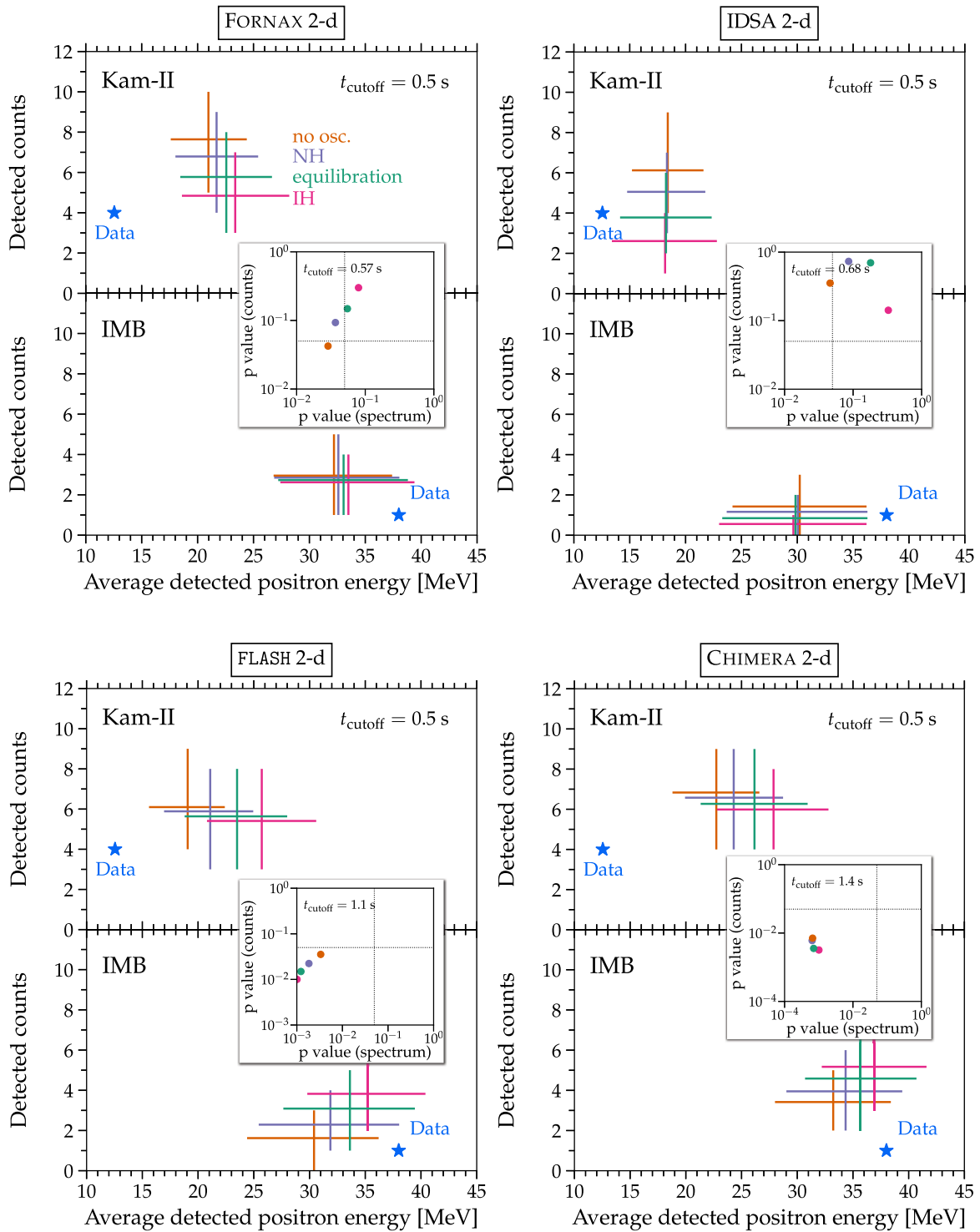
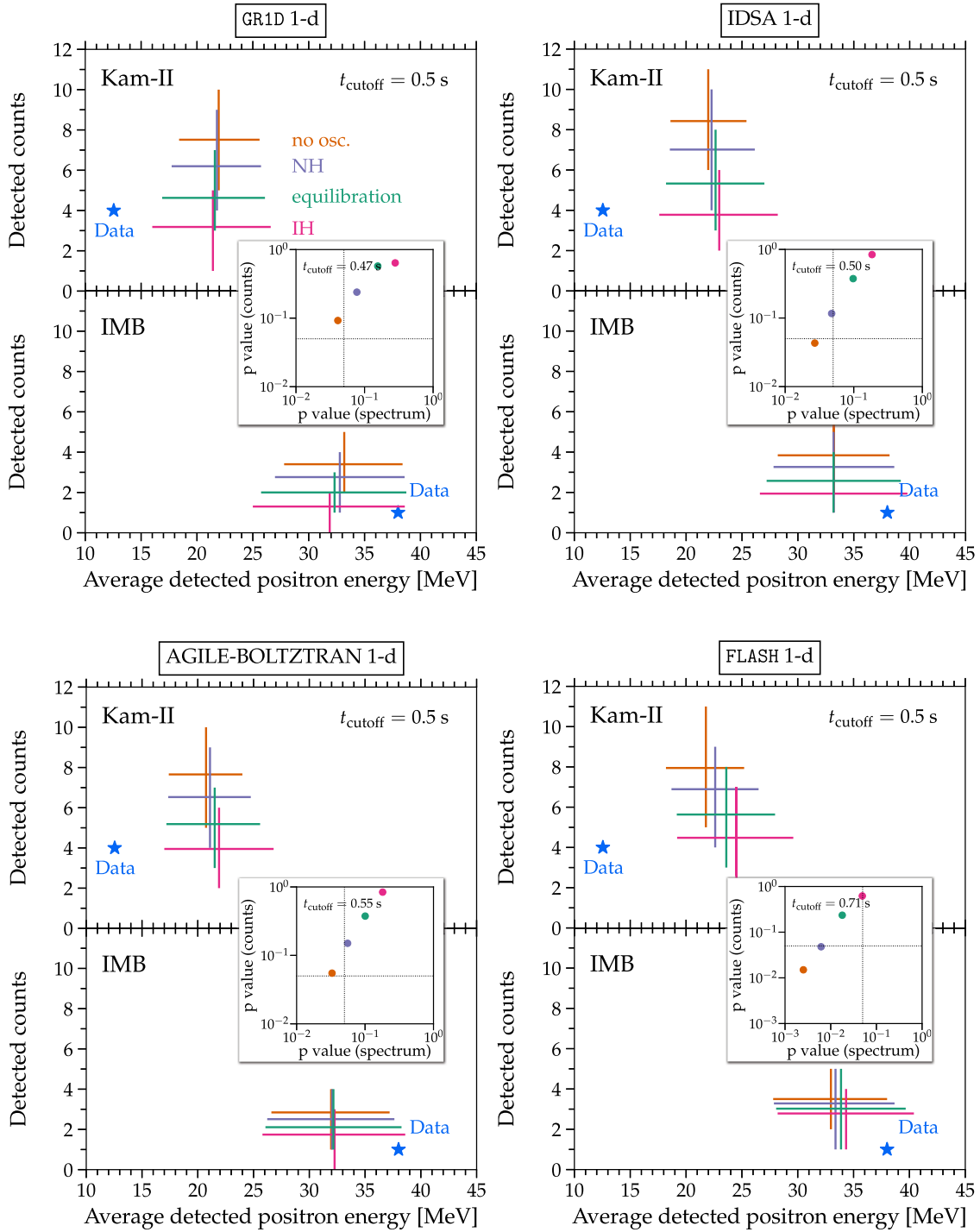FIG. 15.   Different oscillation scenarios for 2-D simulations.

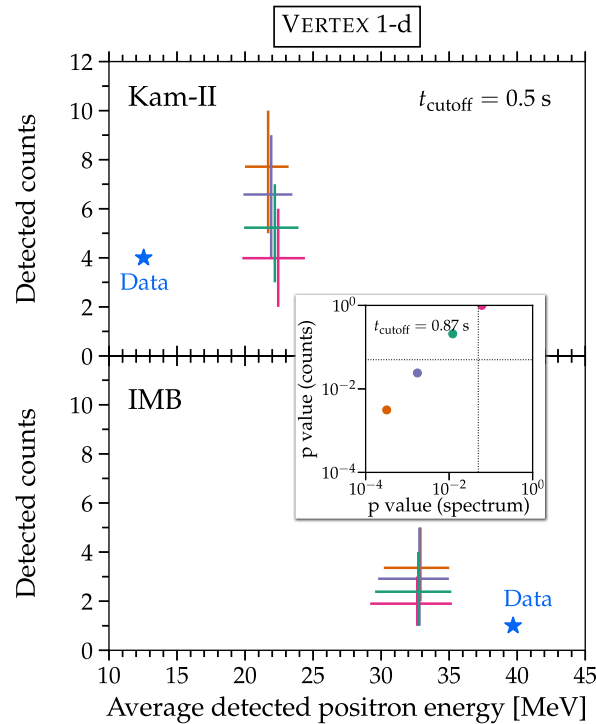FIG. 16.   Different oscillation scenarios for 1-D simulations.

FIG. 17. Figure 16 continued.

on the blue dashed curve. With oscillations, because of the lower flux, we would generally sample fewer events for the mock data samples, which would increase the mock test statistic because of the coarse steps. In combination, it is not clear whether the spectrum p-value would increase or decrease, but what seems to happen in most of the models is that the spectrum p-values end up increasing because they are dominated by the bad fit due to the counts.

[1] K. Hirata *et al.* (Kamiokande-II Collaboration), Observation of a neutrino burst from the supernova SN 1987a, Phys. Rev. Lett. **58,** 1490 (1987).

[2] K. S. Hirata *et al.*, Observation in the Kamiokande-II detector of the neutrino burst from supernova SN 1987a, Phys. Rev. D **38,** 448 (1988).

[3] R. M. Bionta *et al.*, Observation of a neutrino burst in coincidence with supernova SN 1987a in the large magellanic cloud, Phys. Rev. Lett. **58,** 1494 (1987).

[4] C. B. Bratton *et al.* (IMB Collaboration), Angular distribution of events from SN1987a, Phys. Rev. D **37,** 3361 (1988).

[5] W. D. Arnett, John N. Bahcall, R. P. Kirshner, and S. E. Woosley, Supernova 1987A, Annu. Rev. Astron. Astrophys. **27,** 629 (1989).

[6] Richard McCray, Supernova 1987A revisited., Annu. Rev. Astron. Astrophys. **31,** 175 (1993).

[7] Kate Scholberg, Supernova neutrino detection, Annu. Rev. Nucl. Part. Sci. **62,** 81 (2012).

[8] Scott M. Adams, C. S. Kochanek, John F. Beacom, Mark R. Vagins, and K. Z. Stanek, Observing the next galactic supernova, Astrophys. J. **778,** 164 (2013).

[9] Alessandro Mirizzi, Irene Tamborra, Hans-Thomas Janka, Ninetta Saviano, Kate Scholberg, Robert Bollig, Lorenz Hudepohl, and Sovan Chakraborty, Supernova neutrinos: Production, oscillations and detection, Riv. Nuovo Cimento **39,** 1 (2016).

[10] Ko Nakamura, Shunsaku Horiuchi, Masaomi Tanaka, Kazuhiro Hayama, Tomoya Takiwaki, and Kei Kotake, Multimessenger signals of long-term core-collapse supernova simulations: Synergetic observation strategies, Mon. Not. R. Astron. Soc. **461,** 3296 (2016).

[11] Roland Diehl *et al.*, Radioactive Al-26 and massive stars in the galaxy, Nature (London) **439,** 45 (2006).

[12] Weidong Li, Ryan Chornock, Jesse Leaman, Alexei V. Filippenko, Dovi Poznanski, Xiaofeng Wang, Mohan Ganeshalingam, and Filippo Mannucci, Nearby supernova rates from the Lick Observatory Supernova Search—III. The rate-size relation, and the rates as a function of galaxy Hubble type and colour, Mon. Not. R. Astron. Soc. **412,** 1473 (2011).

[13] Karolina Rozwadowska, Francesco Vissani, and Enrico Cappellaro, On the rate of core collapse supernovae in the Milky Way, New Astron. **83,** 101498 (2021).

[14] Florian Hanke, Bernhard Müller, Annop Wongwathanarat, Andreas Marek, and Hans-Thomas Janka, SASI activity in three-dimensional neutrino-hydrodynamics simulations of supernova cores, Astrophys. J. **770,** 66 (2013).

[15] Tomoya Takiwaki, Kei Kotake, and Yudai Suwa, A comparison of two- and three-dimensional neutrino-hydrodynamics simulations of core-collapse supernovae, Astrophys. J. **786,** 83 (2014).

[16] Eric J. Lentz, Stephen W. Bruenn, W. Raphael Hix, Anthony Mezzacappa, O. E. Bronson Messer, Eirik Endeve, John M. Blondin, J. Austin Harris, Pedro Marronetti, and Konstantin N. Yakunin, Three-dimensional core-collapse supernova simulated using a $15M_\odot$ progenitor, Astrophys. J. Lett. **807,** L31 (2015).

[17] H. Thomas Janka, Tobias Melson, and Alexander Summa, Physics of core-collapse supernovae in three dimensions: A sneak preview, Annu. Rev. Nucl. Part. Sci. **66,** 341 (2016).

[18] Evan O'Connor *et al.*, Global comparison of core-collapse supernova simulations in spherical symmetry, J. Phys. G **45,** 104001 (2018).

[19] Stephen W. Bruenn, Anthony Mezzacappa, W. Raphael Hix, Eric J. Lentz, O. E. Bronson Messer, Eric J. Lingerfelt, John M. Blondin, Eirik Endeve, Pedro Marronetti, and Konstantin N. Yakunin, Axisymmetric *ab initio* core-collapse supernova simulations of 12–$25M_\odot$ stars, Astrophys. J. Lett. **767,** L6 (2013).

[20] Stephen W. Bruenn *et al.*, The development of explosions in axisymmetric *ab initio* core-collapse supernova simulations of $12 - 25M_\odot$ stars, Astrophys. J. **818,** 123 (2016).

[21] Evan P. O'Connor and Sean M. Couch, Two dimensional core-collapse supernova explosions aided by general relativity with multidimensional neutrino transport, Astrophys. J. **854,** 63 (2018).

[22] Alexander Summa, Florian Hanke, Hans-Thomas Janka, Tobias Melson, Andreas Marek, and Bernhard Müller, Progenitor-dependent explosion dynamics in self-consistent, axisymmetric simulations of neutrino-driven core-collapse supernovae, Astrophys. J. **825,** 6 (2016).

[23] Kei Kotake, Tomoya Takiwaki, Tobias Fischer, Ko Nakamura, and Gabriel Martínez-Pinedo, Impact of neutrino opacities on core-collapse supernova simulations, Astrophys. J. **853,** 170 (2018).

[24] David Vartanyan, Adam Burrows, David Radice, M. Aaron Skinner, and Joshua Dolence, Revival of the fittest: Exploding core-collapse supernovae from 12 to $25M_\odot$, Mon. Not. R. Astron. Soc. **477,** 3091 (2018).

[25] C. D. Ott, L. F. Roberts, A. da Silva Schneider, J. M. Fedrow, R. Haas, and E. Schnetter, The progenitor dependence of core-collapse supernovae from three-dimensional simulations with progenitor models of 12–$40M_\odot$, Astrophys. J. Lett. **855,** L3 (2018).

[26] Evan P. O'Connor and Sean M. Couch, Exploring fundamentally three-dimensional phenomena in high-fidelity simulations of core-collapse supernovae, Astrophys. J. **865,** 81 (2018).

[27] Robert Glas, Oliver Just, H. Thomas Janka, and Martin Obergaulinger, Three-dimensional core-collapse supernova simulations with multidimensional neutrino transport compared to the ray-by-ray-plus approximation, Astrophys. J. **873,** 45 (2019).

[28] Adam Burrows, David Radice, David Vartanyan, Hiroki Nagakura, M. Aaron Skinner, and Joshua Dolence, The overarching framework of core-collapse supernova explosions as revealed by 3D Fornax simulations, Mon. Not. R. Astron. Soc. **491,** 2715 (2020).

[29] Evan O'Connor and Christian D. Ott, The progenitor dependence of the pre-explosion neutrino emission in core-collapse supernovae, Astrophys. J. **762,** 126 (2013).

[30] Jackson Olsen and Yong-Zhong Qian, Comparison of simulated neutrino emission models with data on supernova 1987A, Phys. Rev. D **104,** 123020 (2021).

[31] S. E. Woosley, Philip A. Pinto, and L. Ensman, Supernova 1987A: Six weeks later, Astrophys. J. **324,** 466 (1988).

[32] Damiano F. G. Fiorillo, Malte Heinlein, Hans-Thomas Janka, Georg Raffelt, Edoardo Vitagliano, and Robert Bollig, Supernova simulations confront SN 1987A neutrinos, Phys. Rev. D **108,** 083040 (2023).

[33] Anthony Mezzacappa, Ascertaining the core collapse supernova mechanism: The state of the art and the road ahead, Annu. Rev. Nucl. Part. Sci. **55,** 467 (2005).

[34] Stephen J. Smartt, Progenitors of core-collapse supernovae, Annu. Rev. Astron. Astrophys. **47,** 63 (2009).

[35] Hans-Thomas Janka, Explosion mechanisms of core-collapse supernovae, Annu. Rev. Nucl. Part. Sci. **62,** 407 (2012).

[36] Adam Burrows and David Vartanyan, Core-collapse supernova explosion theory, Nature (London) **589,** 29 (2021).

[37] Stirling A. Colgate and Richard H. White, The hydrodynamic behavior of supernovae explosions, Astrophys. J. **143,** 626 (1966).

[38] H. A. Bethe and J. R. Wilson, Revival of a stalled supernova shock by neutrino heating, Astrophys. J. **295,** 14 (1985).

[39] J. A. Pons, S. Reddy, M. Prakash, J. M. Lattimer, and J. A. Miralles, Evolution of protoneutron stars, Astrophys. J. **513,** 780 (1999).

[40] Ken'ichiro Nakazato, Kohsuke Sumiyoshi, Hideyuki Suzuki, Tomonori Totani, Hideyuki Umeda, and Shoichi Yamada, Supernova neutrino light curves and spectra for various progenitor stars: From core collapse to protoneutron star cooling, Astrophys. J. Suppl. Ser. **205,** 2 (2013).

[41] Ken'ichiro Nakazato and Hideyuki Suzuki, Cooling timescale for protoneutron stars and properties of nuclear matter: Effective mass and symmetry energy at high densities, Astrophys. J. **878,** 25 (2019).

[42] Shirley Weishi Li, Luke F. Roberts, and John F. Beacom, Exciting prospects for detecting late-time neutrinos from core-collapse supernovae, Phys. Rev. D **103,** 023016 (2021).

[43] E. N. Alekseev, L. N. Alekseeva, I. V. Krivosheina, and V. I. Volchenko, Detection of the neutrino signal from SN1987A in the LMC using the INR Baksan Underground Scintillation Telescope, Phys. Lett. B **205,** 209 (1988).

[44] Thomas J. Loredo and Don Q. Lamb, Bayesian analysis of neutrinos observed from supernova SN-1987A, Phys. Rev. D **65,** 063002 (2002).

[45] Adam Burrows and James M. Lattimer, Neutrinos from SN 1987A, Astrophys. J. Lett. **318,** L63 (1987).

[46] Stephen W. Bruenn, Neutrinos from SN1987A and current models of stellar-core collapse, Phys. Rev. Lett. **59,** 938 (1987).

[47] Katsuhiko Sato and Hideyuki Suzuki, Analysis of neutrino burst from the supernova 1987A in the Large Magellanic Cloud, Phys. Rev. Lett. **58**, 2722 (1987).

[48] M. L. Pumo, S. P. Cosentino, A. Pastorello, S. Benetti, S. Cherubini, G. Manicò, and L. Zampieri, Long-rising Type II supernovae resembling supernova 1987A—I. A comparative study through scaling relations, Mon. Not. R. Astron. Soc. **521**, 4801 (2023).

[49] W. Hillebrandt, P. Hoeflich, A. Weiss, and J. W. Truran, Explosion of a blue supergiant: A model for supernova SN1987A, Nature (London) **327**, 597 (1987).

[50] S. E. Woosley, P. A. Pinto, P. G. Martin, and Thomas A. Weaver, Supernova 1987A in the large magellanic cloud: The explosion of a approximately 20 M_{sun} star which has experienced mass loss?, Astrophys. J. **318**, 664 (1987).

[51] Hideyuki Saio, Mariko Kato, and Ken'ichi Nomoto, Why did the progenitor of SN 1987A undergo the blue-red-blue evolution?, Astrophys. J. **331**, 388 (1988).

[52] Philipp Podsiadlowski, The progenitor of SN 1987A, Publ. Astron. Soc. Pac. **104**, 717 (1992).

[53] Athira Menon and Alexander Heger, The quest for blue supergiants: Binary merger models for the evolution of the progenitor of SN 1987A, Mon. Not. R. Astron. Soc. **469**, 4649 (2017).

[54] T. Urushibata, K. Takahashi, H. Umeda, and T. Yoshida, A progenitor model of SN 1987A based on the slow-merger scenario, Mon. Not. R. Astron. Soc. **473**, L101 (2018).

[55] Ko Nakamura, Tomoya Takiwaki, and Kei Kotake, Three-dimensional simulation of a core-collapse supernova for a binary star progenitor of SN 1987A, Mon. Not. R. Astron. Soc. **514**, 3941 (2022).

[56] S. E. Woosley and Alexander Heger, Nucleosynthesis and remnants in massive stars of solar metallicity, Phys. Rep. **442**, 269 (2007).

[57] Mathias Th. Keil, Georg G. Raffelt, and Hans-Thomas Janka, Monte Carlo study of supernova neutrino spectra formation, Astrophys. J. **590**, 971 (2003).

[58] Beat Jegerlehner, Frank Neubig, and Georg Raffelt, Neutrino oscillations and the supernova SN1987A signal, Phys. Rev. D **54**, 1194 (1996).

[59] Cecilia Lunardini and Alexei Yu. Smirnov, Neutrinos from SN1987A: Flavor conversion and interpretation of results, Astropart. Phys. **21**, 703 (2004).

[60] Maria Laura Costantini, Aldo Ianni, Giulia Pagliaroli, and Francesco Vissani, Is there a problem with low energy SN1987A neutrinos?, J. Cosmol. Astropart. Phys. 05 (2007) 014.

[61] G. Pagliaroli, F. Vissani, M. L. Costantini, and A. Ianni, Improved analysis of SN1987A antineutrino events, Astropart. Phys. **31**, 163 (2009).

[62] Francesco Vissani, Comparative analysis of SN1987A antineutrino fluence, J. Phys. G **42**, 013001 (2015).

[63] P. Vogel and John F. Beacom, Angular distribution of neutron inverse beta decay, $\bar{\nu}_e + p \rightarrow e^+ + n$, Phys. Rev. D **60**, 053003 (1999).

[64] Alessandro Strumia and Francesco Vissani, Precise quasielastic neutrino/nucleon cross-section, Phys. Lett. B **564**, 42 (2003).

[65] N. Panagia, Distance to SN 1987 A and the LMC, in New Views of the Magellanic Clouds, edited by Y. H. Chu, N. Suntzeff, J. Hesser, and D. Bohlender (Cambridge University Press, 1999), Vol. 190, p. 549.

[66] Hasan Yuksel and John F. Beacom, Neutrino spectrum from SN 1987A and from cosmic supernovae, Phys. Rev. D **76**, 083007 (2007).

[67] Hiroki Nagakura and Kenta Hotokezaka, Non-thermal neutrinos created by shock acceleration in successful and failed core-collapse supernova, Mon. Not. R. Astron. Soc. **502**, 89 (2021).

[68] Huaiyu Duan, George M. Fuller, and Yong-Zhong Qian, Collective neutrino oscillations, Annu. Rev. Nucl. Part. Sci. **60**, 569 (2010).

[69] Shunsaku Horiuchi and James P Kneller, What can be learned from a future supernova neutrino detection?, J. Phys. G **45**, 043002 (2018).

[70] Irene Tamborra and Shashank Shalgar, New developments in flavor evolution of a dense neutrino gas, Annu. Rev. Nucl. Part. Sci. **71**, 165 (2021).

[71] Francesco Capozzi and Ninetta Saviano, Neutrino flavor conversions in high-density astrophysical and cosmological environments, Universe **8**, 94 (2022).

[72] Sherwood Richers and Manibrata Sen, Fast flavor transformations, arXiv:2207.03561.

[73] Amol S. Dighe and Alexei Yu. Smirnov, Identifying the neutrino mass spectrum from the neutrino burst from a supernova, Phys. Rev. D **62**, 033007 (2000).

[74] Jakob Ehring, Sajad Abbar, Hans-Thomas Janka, Georg Raffelt, and Irene Tamborra, Fast neutrino flavor conversion in core-collapse supernovae: A parametric study in 1D models, Phys. Rev. D **107**, 103034 (2023).

[75] Hiroki Nagakura, Roles of fast neutrino-flavor conversion on the neutrino-heating mechanism of core-collapse supernova, Phys. Rev. Lett. **130**, 211401 (2023).

[76] Jakob Ehring, Sajad Abbar, Hans-Thomas Janka, Georg Raffelt, and Irene Tamborra, Fast neutrino flavor conversions can help and hinder neutrino-driven explosions, Phys. Rev. Lett. **131**, 061401 (2023).

[77] S. E. Woosley, J. R. Wilson, and R. Mayle, Gravitational collapse and the cosmic antineutrino background, Astrophys. J. **302**, 19 (1986).

[78] David Vartanyan, Adam Burrows, David Radice, Aaron M. Skinner, and Joshua Dolence, A successful 3D core-collapse supernova explosion model, Mon. Not. R. Astron. Soc. **482**, 351 (2019).

[79] Adam Burrows, David Radice, and David Vartanyan, Three-dimensional supernova explosion simulations of 9-, 10-, 11-, 12-, and 13-$M_\odot$ stars, Mon. Not. R. Astron. Soc. **485**, 3153 (2019).

[80] David Vartanyan, Adam Burrows, and David Radice, Temporal and angular variations of 3D core-collapse supernova emissions and their physical correlations, Mon. Not. R. Astron. Soc. **489**, 2227 (2019).

[81] Hiroki Nagakura, Adam Burrows, David Radice, and David Vartanyan, Towards an understanding of the resolution dependence of core-collapse supernova simulations, Mon. Not. R. Astron. Soc. **490**, 4622 (2019).

[82] MacKenzie L. Warren, Sean M. Couch, Evan P. O'Connor, and Viktoriya Morozova, Constraining properties of the next nearby core-collapse supernova with multimessenger signals, Astrophys. J. **898**, 139 (2020).

[83] Amanda L. Baxter *et al.* (SNEWS Collaboration), SNEWPY: A data pipeline from supernova simulations to neutrino signals, Astrophys. J. **925,** 107 (2022).

[84] Irene Tamborra, Georg Raffelt, Florian Hanke, Hans-Thomas Janka, and Bernhard Müller, Neutrino emission characteristics and detection opportunities based on three-dimensional supernova simulations, Phys. Rev. D **90,** 045032 (2014).

[85] Tomoya Takiwaki and Kei Kotake, Anisotropic emission of neutrino and gravitational-wave signals from rapidly rotating core-collapse supernovae, Mon. Not. R. Astron. Soc. **475,** L91 (2018).

[86] Zidu Lin, Cecilia Lunardini, Michele Zanolin, Kei Kotake, and Colter Richardson, Detectability of standing accretion shock instabilities activity in supernova neutrino signals, Phys. Rev. D **101,** 123028 (2020).

[87] Laurie Walk, Irene Tamborra, Hans-Thomas Janka, and Alexander Summa, Effects of the standing accretion-shock instability and the lepton-emission self-sustained asymmetry in the neutrino emission of rotating supernovae, Phys. Rev. D **100,** 063018 (2019).

[88] Robert Bollig, Naveen Yadav, Daniel Kresse, H. Th. Janka, Bernhard Müller, and Alexander Heger, Self-consistent 3D supernova models from −7 minutes to +7 s: A 1-bethe explosion of a ∼19$M_\odot$ progenitor, Astrophys. J. **915,** 28 (2021).

[89] Adam Burrows (private communication).

[90] R. Farmer, C. E. Fields, I. Petermann, Luc Dessart, M. Cantiello, B. Paxton, and F. X. Timmes, On variations of pre-supernova model properties, Astrophys. J. Suppl. Ser. **227,** 22 (2016).

[91] Tuguldur Sukhbold, T. Ertl, S. E. Woosley, Justin M. Brown, and H. T. Janka, Core-collapse supernovae from 9 to 120 solar masses based on neutrino-powered explosions, Astrophys. J. **821,** 38 (2016).

[92] Luke F. Roberts and Sanjay Reddy, Neutrino signatures from young neutron stars, in *Handbook of Supernovae* (Springer, Cham, 2017).

[93] Frederick James, *Statistical Methods in Experimental Physics* (World Scientific, Singapore, 2006).